CP violation in $b \to s\ell\ell$: A model independent analysis

Neetu Raj Singh Chundawat*

Indian Institute of Technology Jodhpur, Jodhpur 342037, India

(Received 8 March 2023; accepted 28 March 2023; published 17 April 2023)

We perform a model-independent global fit to all germane and updated $b \to s\ell\ell$ ($\ell = e, \mu$) data assuming new physics couplings to be complex. Under the approximation that new physics universally affects muon and electron sectors and that either one or two related operators contribute at a time, we identify scenarios which provide a good fit to the data. It turns out that the favored scenarios remain the same as obtained for the real fit. Further, the magnitude of complex couplings can be as large as that of their real counterparts and these are reflected in the predictions of the direct *CP* asymmetry, A_{CP}, in $B \to (K, K^*)\mu^+\mu^-$ along with a number of angular *CP* asymmetries, A_i, in $B^0 \to K^{*0}\mu^+\mu^-$ decay. The sensitivities of these observables to various solutions are different in the low and high-q^2 bins. We also determine observables which can serve as unique identifier for a particular new physics solution. Moreover, we examine correlations between A_{CP} and several A_i observables. A precise measurement of A_{CP} and A_i observables can not only confirm the existence of additional weak phases but can also enable unique determination of Lorentz structure of possible new physics in $b \to s\mu^+\mu^-$ transition.

DOI: 10.1103/PhysRevD.107.075014

I. INTRODUCTION

One of the key open problems in particle physics is the observed recalcitrant disparity between the amount of matter and antimatter in the Universe. It is expected that the big bang explosion would have created matter and antimatter in equal amounts. However, it is still not understood how one type of matter triumphed over another in the early Universe. Sakharov's conditions provide three necessary ingredients required to create the observed baryon asymmetry [1]. One of these conditions requires a *CP* violation which can be generated through a complex phase in the Lagrangian that cannot be reabsorbed through the rephasing of the apposite fields.

The SM of electroweak interactions allows for *CP* violations owing to a complex phase in the quark mixing matrix. The 3×3 CKM matrix can be parametrized by three angles and a single complex phase. This single phase of the CKM matrix is the only source of *CP* violation in the SM. This phase evinces itself in several observables in the decays of K and B mesons. In fact, the *BABAR* and Belle experiments established the CKM paradigm of *CP* violation through several measurements of observables in the decays of B mesons. However, unlike parity violation, which is maximal, the observed *CP* violation is small and cannot account for the observed baryon asymmetry. The amount of predicted baryons in the Universe using the CKM formalism falls several orders of magnitude short of the observed value. Therefore one needs to explore beyond the CKM paradigm of the SM.

The *CP* violating observables in the decays induced by the quark level transition $b \to s\mu^+\mu^-$ are particularly important in probing new physics. see for, e.g., [2–11]. This is because these observables are highly suppressed in the SM, i.e., they are predicted to be less than a percent level in the SM [2,3]. Even after including the next-to-leading order QCD corrections and hadronic uncertainties, the *CP* asymmetries are not expected to transcend 1% [4–6]. The *CP*-violating observables can be measured at LHC or at Belle-II provided new physics enhances them to a level of a few percent. Therefore measurement of any *CP* violating observable in $b \to s\mu^+\mu^-$ sector will provide a luculent signature of new physics.

The decay mode $b \to s\mu^+\mu^-$ is already in spotlight for a decade due to the fact that it has provided a number of observables whose measurements are in contention with the predictions of the SM. These include number of observables in $B_s \to \phi\mu^+\mu^-$ and $B \to K^*\mu^+\mu^-$ decays which are related only to the muon sector. For, e.g., the experimental value of the branching ratio of $B_s \to \phi\mu^+\mu^-$ decay ostentates tension with the SM at 3.5σ level [12,13]. The measurement of the optimized angular observable P_5' in $B \to K^*\mu^+\mu^-$ decay in the ($4.0\ \text{GeV}^2 \le q^2 \le 6.0\ \text{GeV}^2$) bin deviates from the SM

*chundawat.1@iitj.ac.in

prediction at the level of 3σ [14–19].[1] The measured value of the branching ratio of the decay $B_s \to \mu^+\mu^-$ also regaled tension with the SM at 2σ level [24–28]. However, the CMS collaboration recently updated the measurement of the branching ratio of $B_s \to \mu^+\mu^-$ [29] using the full Run 2 dataset. This resulted in a new world average of the branching ratio [30] which is now in agreement with its SM prediction [31,32].

The measurement of the ratio $R_K \equiv \Gamma(B^+ \to K^+\mu^+\mu^-)/\Gamma(B^+ \to K^+e^+e^-)$ showed a scantiness of 3.1σ as compared to the SM value in the $(1.1\ \text{GeV}^2 \leq q^2 \leq 6.0\ \text{GeV}^2)$ bin [33–35]. Here q^2 is the dilepton invariant mass-squared. The measurements of analogous ratio, R_{K^*}, in the $(0.045\ \text{GeV}^2 \leq q^2 \leq 1.1\ \text{GeV}^2)$ and $(1.1\ \text{GeV}^2 \leq q^2 \leq 6.0\ \text{GeV}^2)$ bins also nonconcurred with the SM at level of $\sim 2.5\sigma$ [36]. In [37–39], it was shown that these deviations are valid even after including the QED corrections. These contestations, known as lepton flavor universality violation (LFUV) was accredited to new physics in $b \to s\mu^+\mu^-$ or/and $b \to se^+e^-$ decays, i.e., it required nonuniversal couplings in muon and electron sectors. However, on December 20, 2022, the LHCb collaboration updated these measurements [40,41] which are now consistent with the SM predictions. As the updated values of R_K and R_{K^*} are now consistent with their SM predictions, these would force the new physics couplings in electron and muon sectors to be *nearly* universal in nature.

Apart from these LFU ratios, the LHCb collaboration had also provided measurements of new LFU ratios in $B^0 \to K^0_S\mu^+\mu^-$ and $B^+ \to K^{*+}\mu^+\mu^-$ the channels [42]. These measurements concur with the SM at $\sim 1.5\sigma$ level. In the recent updates of R_K and R_{K^*}, the LHCb collaboration included the experimental systematic effects which were absent in the previous analysis [40,41]. Due to this, the updated values are now consistent with SM predictions. Therefore it is expected that the measurements of these new LFU observables would also suffer from the same systematic effects.

In order to determine the Lorentz structure of possible new physics that can accommodate the anomalous measurements in $b \to s\ell\ell$ decays, a model independent analysis can be performed using the language of effective field theory [23,43–57]. Barring a few [48,51], most of these analyses assume new physics Wilson coefficients (WCs) to be real. In this work, we allow the new physics WCs to be complex and perform a global analysis of all CP-conserving $b \to s\ell\ell$ $(\ell = e,\ \mu)$ data under the assumption that the beyond SM contributions affect both the muon as well as electron sector equally. Apart from the updated values of the LFU ratios R_K and R_{K^*} by the LHCb collaboration in December 2022, the branching ratios of $B \to X_s\mu^+\mu^-$, $B^0 \to K^0\mu^+\mu^-$, $B^+ \to K^+\mu^+\mu^-$, $B^0 \to K^{*0}\mu^+\mu^-$, $B^+ \to K^{*+}\mu^+\mu^-$, and $B^0_s \to \phi\mu^+\mu^-$ in several q^2 bins along with $B(B^0_s \to \mu^+\mu^-)$ are included in the fits. Further, we include a number of CP-conserving angular observables in $B^0 \to K^{*0}\mu^+\mu^-$, $B^+ \to K^{*+}\mu^+\mu^-$ and $B^0_s \to \phi\mu^+\mu^-$ decays. Moreover, we also include a number of observables in decays induced by $b \to se^+e^-$ transition. These observables are obtained by averaging over the angular distributions of B and $\bar{B}$ decays.

We take the most frugal approach by considering only one operator or two related operators at a time. For statistically favored scenarios, we then obtain predictions for several CP-violating observables. For $B^+ \to K^+\mu^+\mu^-$ decay, we calculate the direct CP asymmetry, A_{CP}, whereas for $B^0 \to K^{*0}\mu^+\mu^-$ decay, a number of angular CP-asymmetries, A_i's, are analyzed along with A_{CP}. These are obtained by comparing the angular distributions of the corresponding B and $\bar{B}$ decays. For favored new physics solutions, we also study correlations between CP violating angular asymmetries in $B^0 \to K^{*0}\mu^+\mu^-$ decay and A_{CP} which is expected to be measured with the highest statistical significance among all CP asymmetries. These correlations would not only reveal the impact of new physics phase on various quantities but would also help in sequestering between the allowed scenarios.

Plan of the work is as follows. In Sec. II, we discuss the methodology adopted in this work. We then provide the fit results. Using the fit results, we calculate the direct CP asymmetry in $B^+ \to K^+\mu^+\mu^-$ in Sec. III. In the following section, we obtain predictions of a number of CP-violating observables in $B^0 \to K^{*0}\mu^+\mu^-$ decay. We also study correlations between A_{CP} and several CP-violating angular observables related to $B^0 \to K^{*0}\mu^+\mu^-$ decay. Finally, we conclude in Sec. V.

II. A FIT TO ALL $b \to s\ell\ell$ DATA

We start by performing a global fit to all CP conserving data in $b \to s\ell\ell$ $(\ell = e, \mu)$ by assuming new physics WCs to be complex. The data includes the updated measurements of LFU ratios R_K and R^*_K [40,41] along with the branching ratio of $B_s \to \mu^+\mu^-$ [30]. For reasons mentioned in the Introduction, we do not include measurements of new LFU ratios $R_{K^0_S}$, $R_{K^{*+}}$ [42] in the fit. The fit also includes the updated measurements for several $B_s \to \phi\mu^+\mu^-$ observables [13,58]. We closely follow the methodology adopted in [56] where the new physics couplings were assumed to be real. In this section, we intend to espy the following:

(i) The impact of the assumption of the complex coupling on the fit, i.e., to spell out the differences between the real and complex fits by making use of the most updated data.
(ii) The upper limit on the allowed parameter space of the new weak phases accredited by the current data. This will enable us to identify various CP violating

[1]These can also be attributed to under estimation of hadronic uncertainties in the SM such as non factorizable power corrections [20–23].

observables where large enhancement over the SM value is possible.

A. Methodology

We include following CP conserving observables in our fit:

(1) *LFU ratios:* Within the SM, R_K is predicted to be close to unity owing to LFU which is deeply instilled in the symmetry structure of the SM. To be more specific, $R_K^{\rm SM} = 1 \pm 0.01$ [33]. This ratio was first measured in 2014 by the LHCb collaboration [59] in 1.0 GeV$^2 \le q^2 \le$ 6.0 GeV^2 bin and updated in 2021 [35]. The measured value of $R_K^{\rm exp} = 0.846^{+0.044}_{-0.041}$ [35] retrogressed from the SM prediction at the level of 3.1σ. This was considered as an inkling of LFUV.

In 2017, the notion of LFUV in $b \to s\ell\ell$ was substantiated by the observation of the ratio R_{K^*} by the LHCb collaboration [36]. This measurement was performed in two q^2 bins. The measured values

$$R_{K^*}^{\rm exp} = \begin{cases} 0.660^{+0.110}_{-0.070} \pm 0.024, & q^2 \subset [0.045, 1.1], \\ 0.685^{+0.113}_{-0.069} \pm 0.047, & q^2 \subset [1.1, 6.0], \end{cases} \quad (1)$$

detour from the SM predictions [34,60] at the level of $\sim 2.5\sigma$. Apart from LHCb, Belle collaboration also measured R_{K^*} in 0.045 GeV$^2 < q^2 <$ 1.1 GeV^2, 1.1 GeV$^2 < q^2 <$ 6.0 GeV^2, and 15.0 GeV$^2 < q^2 <$ 19.0 GeV^2 bins [61].

In 2021, LHCb also provided measurements of new LFU ratios $R_{K_S^0} \equiv \Gamma(B^0 \to K_S^0 \mu^+\mu^-)/\Gamma(B^0 \to K_S^0 e^+e^-)$ and $R_{K^{*+}} \equiv \Gamma(B^+ \to K^{*+}\mu^+\mu^-)/\Gamma(B^+ \to K^{*+}e^+e^-)$ [42]. The measured value of $R_{K_S^0}^{\rm exp} = 0.66^{+0.20+0.02}_{-0.14-0.04}$ and $R_{K^{*+}}^{\rm exp} = 0.70^{+0.18+0.03}_{-0.13-0.04}$ in 1.1 GeV$^2 \le q^2 \le$ 6.0 GeV^2 bin acquiesces with the SM at 1.5σ level [42].

On December 20, 2022, the LHCb collaboration provided updated measurements of the LFU ratios R_K and R_{K^*}. The measured values are [40,41]:

$$R_K^{\rm exp} = \begin{cases} 0.994^{+0.090}_{-0.082}({\rm stat})^{+0.029}_{-0.027}({\rm sysy}), & q^2 \subset [0.1, 1.1], \\ 0.949^{+0.041}_{-0.041}({\rm stat})^{+0.022}_{-0.022}({\rm sysy}), & q^2 \subset [1.1, 6.0]. \end{cases} \quad (2)$$

$$R_{K^*}^{\rm exp} = \begin{cases} 0.927^{+0.093}_{-0.087}({\rm stat})^{+0.036}_{-0.035}({\rm sysy}), q^2 \subset [0.1, 1.1], \\ 1.027^{+0.072}_{-0.068}({\rm stat})^{+0.027}_{-0.026}({\rm sysy}), q^2 \subset [1.1, 6.0]. \end{cases} \quad (3)$$

It is thus obvious that these values are consistent with their SM predictions. We include these updated measurements in the fit along with the Belle measurements of R_{K^*}. Further, $R_{K_S^0}$ and $R_{K^{*+}}$ measurements are excluded from the fit.

(2) *Branching ratios:* We include the updated world average of the branching ratio of the purely leptonic decay $B_s \to \mu^+\mu^-$ which is $(3.45 \pm 0.29) \times 10^{-9}$ [30]. This average value is in excellent agreement with the SM prediction [31,32]. We also consider the branching fractions of inclusive decay modes $B \to X_s\mu^+\mu^-$ and $B \to X_s e^+e^-$ [62] in the fit in the low and high-q^2 bins.

We also ensheathe measurements of the differential branching fraction of several semileptonic decays. The recently updated measurements of the differential branching fraction of $B_s \to \phi\mu^+\mu^-$ by LHCb in various q^2 intervals are included in the fit [13]. Further, the differential branching ratios of $B^0 \to K^{*0}\mu^+\mu^-$ [63–65], $B^+ \to K^{*+}\mu^+\mu^-$, $B^0 \to K^0\mu^+\mu^-$ and $B^+ \to K^+\mu^+\mu^-$ [65,66] in different q^2 bins are encapsulated in the analysis. In $b \to se^+e^-$ sector, we include measurement of the differential branching fraction of $B^+ \to K^+e^+e^-$ in 1.0 $\le q^2 \le$ 6.0 GeV^2 bin [59].

(3) *Angular observables:* We consider a plentitude of CP conserving $B^0 \to K^{*0}\mu^+\mu^-$ angular observables in the fit. This entails longitudinal polarization fraction F_L, forward-backward asymmetry $A_{\rm FB}$ and observables S_3, S_4, S_5, S_7, S_8, S_9 in various q^2 bins, as measured by the LHCb collaboration [16]. We also include their experimental correlations. We also encompass the angular observables F_L, P_1, P_4', P_5', P_6', and P_8' measured by ATLAS [67] along with P_1, P_5' measured by CMS [68]. Further, the measurements of F_L and $A_{\rm FB}$ by CDF and CMS collaborations are also included [64,65] in our analysis.

We then consider full set of angular observables in the decay $B^+ \to K^{*+}\mu^+\mu^-$ which was measured for the first time by the LHCb collaboration in 2020 [69]. The optimized angular observables $P_1 - P_8'$ and longitudinal polarization fraction F_L, along with their experimental correlations are included in the fit [69]. Finally, we include CP conserving angular observables in $B_s \to \phi\mu^+\mu^-$ decay mode. There are F_L, S_3, S_4, and S_7 as measured by the LHCb in 2021. The available experimental correlations are also subsumed in the fit [58].

In decays induced by $b \to se^+e^-$ transition, we include the longitudinal polarization fraction f_L in the decay $B^0 \to K^{*0}e^+e^-$ in $0.002 \le q^2 \le 1.12$ GeV^2 bin as measured by the LHCb collaboration [70]. Further, we also include P_4' and P_5' measured by the Belle collaboration in $0.1 \le q^2 \le 4$ GeV^2, $1.0 \le q^2 \le 6.0$ GeV^2 and $14.18 \le q^2 \le 19.0$ GeV^2 bins [71].

In order to identify the Lorentz structure of possible new physics that can account for the discrepancies in $b \to s\ell\ell$ data, we perform a model independent analysis within the framework of effective field theory. For this we consider new physics in the form of vector and axial-vector operators. The effective Hamiltonian for $b \to s\ell\ell$ transition is then given by

$$\mathcal{H}_{\rm eff}(b \to s\ell\ell) = \mathcal{H}^{\rm SM} + \mathcal{H}^{\rm VA}. \tag{4}$$

Here the SM effective Hamiltonian can be written as

$$\begin{aligned}\mathcal{H}^{\rm SM} = -\frac{4G_F}{\sqrt{2}\pi} V_{ts}^* V_{tb} \Bigg[& \sum_{i=1}^{6} C_i \mathcal{O}_i + C_8 \mathcal{O}_8 \\ & + C_7 \frac{e}{16\pi^2} [\bar{s}\sigma_{\alpha\beta}(m_s P_L + m_b P_R) b] F^{\alpha\beta} \\ & + C_9^{\rm SM} \frac{\alpha_{\rm em}}{4\pi} (\bar{s}\gamma^\alpha P_L b)(\bar{\ell}\gamma_\alpha \ell) \\ & + C_{10}^{\rm SM} \frac{\alpha_{\rm em}}{4\pi} (\bar{s}\gamma^\alpha P_L b)(\bar{\ell}\gamma_\alpha\gamma_5 \ell) \Bigg],\end{aligned} \tag{5}$$

where V_{ij} are the elements of the Cabibbo-Kobayashi-Maskawa (CKM) matrix. The short-distance contributions are enciphered in the WCs C_i of the four-Fermi operators $\mathcal{O}_i$ where the scale-dependence is implicit, i.e., $C_i \equiv C_i(\mu)$ and $\mathcal{O}_i \equiv \mathcal{O}_i(\mu)$. The operators $\mathcal{O}_i$ $(i = 1, \ldots, 6, 8)$ contribute through the modifications $C_7(\mu) \to C_7^{\rm eff}(\mu, q^2)$ and $C_9(\mu) \to C_9^{\rm eff}(\mu, q^2)$. The new physics effective Hamiltonian can be written as

$$\begin{aligned}\mathcal{H}^{\rm VA} = -\frac{\alpha_{\rm em} G_F}{\sqrt{2}\pi} V_{ts}^* V_{tb} \Big[& C_9^{\rm NP} (\bar{s}\gamma^\alpha P_L b)(\bar{\ell}\gamma_\alpha \ell) \\ & + C_{10}^{\rm NP} (\bar{s}\gamma^\alpha P_L b)(\bar{\ell}\gamma_\alpha\gamma_5 \ell) + C'_9 (\bar{s}\gamma^\alpha P_R b)(\bar{\ell}\gamma_\alpha \ell) \\ & + C'_{10} (\bar{s}\gamma^\alpha P_R b)(\bar{\ell}\gamma_\alpha\gamma_5 \ell) \Big].\end{aligned} \tag{6}$$

Here $C_9^{\rm NP}$, $C_{10}^{\rm NP}$, C'_9, and C'_{10} are the new physics WCs which are assumed to be complex in the current analysis. Following a penurious approach, we ruminate only those scenarios where either only one new physics operator or two operators whose WCs are linearly related, contributes. We call them as "1D" scenarios. Under this assumption, we perform a χ^2 fit to identify solutions which can accommodate the current $b \to s\ell\ell$ measurements. The fit is performed using the CERN minimization code Minuit [72]. The χ^2 which is a function of new physics WCs is defined as

$$\chi^2(C_i, C_j) = [\mathcal{O}_{\rm th}(C_i, C_j) - \mathcal{O}_{\rm exp}]^T \mathcal{C}^{-1} [\mathcal{O}_{\rm th}(C_i, C_j) - \mathcal{O}_{\rm exp}], \tag{7}$$

where $\mathcal{O}_{\rm th}(C_i, C_j)$ are the theoretical predictions of the N = 179 observables used in the fit and $\mathcal{O}_{\rm exp}$ are the corresponding central values of the experimental measurements. The total $N \times N$ covariance matrix is obtained by adding the individual theoretical and experimental covariance matrices. The theoretical predictions of N = 179 observables along with the theoretical covariance matrix are evaluated using FLAVIO [60] where the observables are preimplemented based on Refs. [73,74]. The experimental correlations, $\mathcal{O}_{\rm exp}$, are admitted for the angular observables in $B^0 \to K^{*0}\mu^+\mu^-$ [16], $B^+ \to K^{*+}\mu^+\mu^-$ [69] and $B_s \to \phi\mu^+\mu^-$ [58]. Further, for asymmetric errors, we use the larger error on both sides of the central value.

The χ^2 value in the SM is represented by $\chi^2_{\rm SM}$ whereas $\chi^2_{\rm bf}$ represents the value at the best-fit point in the presence of new physics. We then quantify the goodness of fit by $\Delta\chi^2 \equiv \chi^2_{\rm SM} - \chi^2_{\rm bf}$ for each new physics scenario. This means that, under the given assumptions, the largest value of this quantity would represent the best possible new physics scenario to accommodate the entire $b \to s\ell\ell$ data.

B. Fit results

The fit results are presented in Table I. For comparison, we provide the updated fit results for the real WCs. Using the values of R_K and R_{K^*} along with the measurement of LFU ratios $R_{K_s^0}$ & $R_{K^{*+}}$ [42] and older world average of the branching ratio of $B_s \to \mu^+\mu^-$ [50], it was well established

TABLE I. The best fit values of new WCs in various 1D scenarios. Here $\Delta\chi^2 = \chi^2_{\rm SM} - \chi^2_{\rm bf}$ where $\chi^2_{\rm bf}$ is the χ^2 at the best fit point and $\chi^2_{\rm SM}$ corresponds to the SM which is $\chi^2_{\rm SM} \approx 184$.

	Real		Complex	
Wilson coefficient(s)	Best fit value(s)	$\Delta\chi^2_{\rm real}$	1σ range [Re(C_i), Im(C_i)]	$\Delta\chi^2_{\rm complex}$
$C_i = 0$ (SM)	⋯	0	⋯	0
1D scenarios:				
$C_9^{\rm NP}$	-1.08 ± 0.18	27.90	$[(-1.34, -0.80), (-0.86, 0.93)]$	27.91
$C_{10}^{\rm NP}$	0.35 ± 0.15	5.80	$[(0.24, 0.99), (-2.09, 2.08)]$	7.64
$C_9^{\rm NP} = -C_{10}^{\rm NP}$	-0.50 ± 0.12	18.85	$[(-0.83, -0.32), (-1.21, 1.31)]$	18.91
$C_9^{\rm NP} = -C'_9$	0.88 ± 0.16	26.92	$[(-1.12, -0.66), (-0.88, 0.89)]$	28.10

that for real WCs, the new physics solutions $C_9^{\rm NP}$ and $C_9^{\rm NP} = -C_{10}$ provided a good fit to the data whereas $C_9^{\rm NP} = -C_9'$ scenario provided a moderate fit, see for, e.g., [52,56]. In [56], it was shown that $C_{10}^{\rm NP}$ scenario also provided a moderate fit to the data at par with $C_9^{\rm NP} = -C_9'$ solution. It is perspicuous from Table I that the updated fit for real WCs still prefers $C_9^{\rm NP}$ scenario. The $C_9^{\rm NP} = -C_9'$ solution which provided a moderate fit to the older data now provides a good fit at par with $C_9^{\rm NP}$ solution. However, the value of $\Delta\chi^2$ for $C_9^{\rm NP} = -C_{10}$ scenario falls considerably, $\sim$10 below $\Delta\chi^2$ for $C_9^{\rm NP}$ solution. Therefore the $C_9^{\rm NP} = -C_{10}$ scenario can only provide a moderate fit to the current $b \to s\ell\ell$ data. The situation appears to be more grim for $C_{10}^{\rm NP}$ scenario which fails to provide useful improvement in the value of χ^2 as compared to the $\chi^2_{\rm SM}$. This is mainly due to the fact the current world average of the branching ratio of $B_s \to \mu^+\mu^-$ is now in excellent agreement with the SM value.

It is also apparent from Table I that the scenarios that are favored by assuming new physics WCs to be real, remains the preferred ones even for the complex couplings. The $C_9^{\rm NP}$ and $C_9^{\rm NP} = -C_9'$ scenarios turn out to be the most viable scenarios to accommodate all $b \to s\ell\ell$ data whereas the $C_9^{\rm NP} = -C_{10}$ scenario can only provide a moderate fit to the current data. The $C_{10}^{\rm NP}$ scenario has the lowest value of $\Delta\chi^2$ in comparison to the other three solutions. Hence we drop this from further consideration in this work. Further, the imaginary part of all WCs are allowed to have values similar to that of their real counterparts. This is also evident from the 1σ range of complex WCs shown in Fig. 1. Therefore, it will be intriguing to see whether some of the

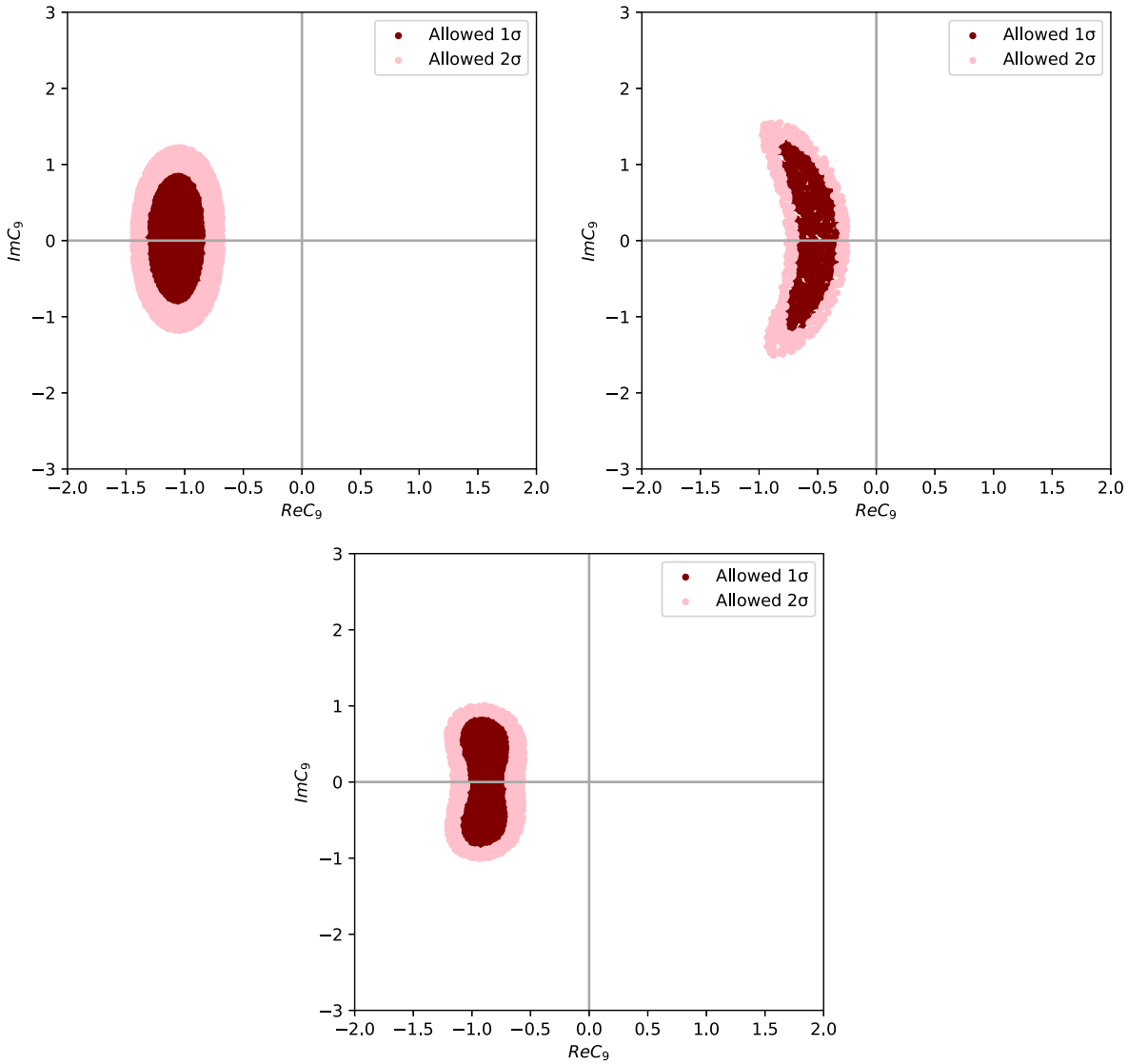

FIG. 1. Allowed parameter space for new physics Scenarios $C_9^{\rm NP}$ (upper left panel), $C_9^{\rm NP} = -C_{10}$ (upper right panel) and $C_9^{\rm NP} = -C_9'$ (lower panel).

CP violating observables can be enhanced up to the current or planned sensitivity of LHCb or Belle-II.

III. DIRECT *CP* ASYMMETRY IN $B^+ \to K^+\mu^+\mu^-$

The *CP* violation can be classified into two types: the direct *CP* asymmetries and triple product *CP* asymmetries:

(i) The direct *CP* asymmetries involve the difference of rates of B and $\bar{B}$, i.e., the direct *CP* violation implies $\Gamma(B \to f) \neq \Gamma(\bar{B} \to \bar{f})$. Assume that there are two contributions, $A_1 \propto e^{i\alpha_1}e^{i\beta_1}$ and $A_2 \propto e^{i\alpha_2}e^{i\beta_2}$, in $B \to f$ decay. Here $\alpha_{1,2}$ and $\beta_{1,2}$ are weak and strong phases, respectively. Then the direct *CP* asymmetry is proportional to $\sin(\alpha_1 - \alpha_2)\sin(\beta_1 - \beta_2)$. This implies that these types of asymmetries can have nonzero values only if the two interfering amplitudes have a relative weak as well as strong phase.

(ii) For a B meson decaying into at least four particles in the final state, T-odd triple products of the form $\vec{p}_i \cdot (\vec{p}_j \times \vec{p}_k)$ where the T-transformation reverses the sign of all particle momenta and spins can appear in the expression of $|A(B \to f)|^2$. Here $\vec{p}_i$'s are the three momenta of the final state particles. The effects of *CP* violation can be captured by comparing the triple products in $B \to f$ and its *CP* conjugate process $\overline{B} \to \bar{f}$. These T-odd *CP* asymmetries are proportional to $\sin(\alpha_1 - \alpha_2)\cos(\beta_1 - \beta_2)$ implying that a relative weak phase between the amplitudes is sufficient to provide a nonzero value. Therefore such asymmetries would display maximal sensitivity to the *CP* violation in the limit of vanishing or very small strong phases.

For $B \to K\mu^+\mu^-$ decay, we only have direct *CP* asymmetry, A_{CP}, which is defined as

$$A_{CP} = \frac{\Gamma - \bar{\Gamma}}{\Gamma + \bar{\Gamma}} \tag{8}$$

where Γ and $\bar{\Gamma}$ are the decay rates of $B^+ \to K^+\mu^+\mu^-$ and $\bar{B} \to \bar{K}\mu^+\mu^-$ decays. $\bar{\Gamma}$ is obtained from Γ by changing the sign of the weak phases. The sign of strong phases remain unchanged. The theoretical expression of $\Gamma(B \to K\mu^+\mu^-)$ is provided in Appendix A.

Effectively, various contributions to $b \to s\mu^+\mu^-$ decay are proportional to CKM factors $V_{tb}^*V_{ts}$ and $V_{ub}^*V_{us}$. The term proportional to $V_{cb}^*V_{cs}$ is eliminated using the unitarity of the CKM mixing matrix. Although the phase of $V_{ub}^*V_{us}$ is large but its magnitude is suppressed in comparison to $V_{tb}^*V_{ts}$. Therefore, within the SM, various contributions to $b \to s\mu^+\mu^-$ have almost similar weak phase. Further, the $c\bar{c}$ and $u\bar{u}$ quark loop generate strong phase in the WC C_9^{eff}. However, this is not substantial and hence the *CP* asymmetries in $b \to s\mu^+\mu^-$ are highly suppressed within the SM. The fact that the new physics strong phase is negligibly small, one requires a large value of new physics weak phase to provide an enhancement at the level of few percent [75].

Including the dielectron mode, the Belle and *BABAR* collaborations measured direct *CP* asymmetries in $B^+ \to K^+\ell\ell$ and $B^0 \to K^{*0}\ell\ell$ decay modes. Based on a data sample of 657 million $B\bar{B}$ pairs, Belle reported A_{CP} in $B^+ \to K^+\ell\ell$ and $B^0 \to K^{*0}\ell\ell$ to be 0.04 ± 0.10 and -0.10 ± 0.10, respectively [76]. These values for *BABAR* collaboration are -0.03 ± 0.14 and 0.03 ± 0.13, respectively [77]. This corresponds to a sample of 471 million $B\bar{B}$ events. These asymmetries, in the muonic channel, were measured by the LHCb collaboration by making use of a dataset corresponding to an integrated luminosity of 3.0 fb^{-1} collected in 2011 and 2012 at center of mass energies of 7 and 8 TeV, respectively. The measured values are $A_{CP}(B^+ \to K^+\ell\ell) = 0.012 \pm 0.017$ and $A_{CP}(B^0 \to K^{*0}\ell\ell) = -0.035 \pm 0.024$ [78–80]. The quoted values are in the full-q^2 region. Owing to large errors, these measurements are consistent with the SM. But on the other hand, a possibility of A_{CP} at a level of a few percent is not ruled out. It would be interesting to see whether such an enhancement is allowed by the current data.

The predictions of A_{CP} in $B^+ \to K^+\mu^+\mu^-$ for all 1D favored solutions are given in Table II. It is apparent that none of the new physics solutions can enhance A_{CP}^K in the low-q^2 bin at the level of a few percent. However, such an enhancement is feasible in the high-q^2 region for C_9^{NP} and $C_9^{NP} = -C_{10}^{NP}$ solutions, the enhancement being more prominent for the later solution. Therefore any observation of A_{CP} in $B^+ \to K^+\mu^+\mu^-$ can be attributed to either of these solutions. The $C_9^{NP} = -C_9'$ scenario predicts $A_{CP}^K < 1\%$.

Here one should emphasize that although the enhancement in the high-q^2 bin is more prominent, the measurement of A_{CP} in the low-q^2 region appears to be more attractive as the branching ratio in the low-q^2 region is larger as compared to the high-q^2 bin. Belle-II experiment is expected to collect a sample of a few thousand events of $B \to (K, K^*)\mu^+\mu^-$ [81]. With such an event sample, it would be possible to have a 3σ determination of the *CP* asymmetries which are of a few percent level.

TABLE II. Predictions of A_{CP} in $B^+ \to K^+\mu^+\mu^-$ decay (1σ range). Here $A_{CP}^K \equiv A_{CP}(B^+ \to K^+\mu^+\mu^-)$.

Wilson coefficients	$A_{CP[1-6]}^K$ (%)	$A_{CP[15-19]}^K$ (%)
$C_i = 0$ (SM)	≈0	≈0
1D scenarios:		
C_9^{NP}	$(-0.33, 0.58)$	$(-3.53, 3.54)$
$C_9^{NP} = -C_{10}^{NP}$	$(-0.52, 0.85)$	$(-5.24, 5.35)$
$C_9^{NP} = -C_9'$	(0.12, 0.12)	$(-0.16, -0.16)$

IV. CP VIOLATING OBSERVABLES IN $B^0 \to K^{*0}\mu^+\mu^-$

The differential distribution of $B \to K^*(\to K\pi)\mu^+\mu^-$ decay can be parametrized in terms of one kinematic and three angular variables. The kinematic variable is $q^2 = (p_B - p_{K^*})^2$, where p_B and p_{K^*} are the four-momenta of B and K^* mesons, respectively. The angular variables are usually defined in the rest frame of the vector meson K^*. These angles are

(i) θ_K the angle between B and K mesons where K meson emerges from the decay of a K^*,
(ii) θ_μ the angle between μ^- and B momenta,
(iii) ϕ the angle between K^* decay plane and the plane defined by the $\mu^+ - \mu^-$ momenta.

The four-fold decay distribution can be expounded as [4,5]

$$\frac{d^4\Gamma}{dq^2 d\cos\theta_\mu d\cos\theta_K d\phi} = \frac{9}{32\pi} I(q^2, \theta_\mu, \theta_K, \phi), \quad (9)$$

where

$$\begin{aligned} I(q^2, \theta_\mu, \theta_K, \phi) = {} & I_1^s \sin^2\theta_K + I_1^c \cos^2\theta_K + (I_2^s \sin^2\theta_K + I_2^c \cos^2\theta_K)\cos 2\theta_\mu + I_3 \sin^2\theta_K \sin^2\theta_\mu \cos 2\phi \\ & + I_4 \sin 2\theta_K \sin 2\theta_\mu \cos\phi + I_5 \sin 2\theta_K \sin\theta_\mu \cos\phi + I_6^s \sin^2\theta_K \cos\theta_\mu \\ & + I_7 \sin 2\theta_K \sin\theta_\mu \sin\phi + I_8 \sin 2\theta_K \sin 2\theta_\mu \sin\phi + I_9 \sin^2\theta_K \sin^2\theta_\mu \sin 2\phi. \end{aligned} \quad (10)$$

The expressions of these twelve angular coefficients $I_i^{(a)}$ [2,5,82] are provided in Appendix B. These coefficients depend on the q^2 variable and on various hadronic form factors. The corresponding expression for the four-fold decay distribution of the CP conjugate decay mode can be obtained by substituting θ_μ by $(\pi - \theta_\mu)$ and ϕ by $-\phi$. This results in the following transformations of angular coefficients

$$I^{(a)}_{1,2,3,4,7} \Rightarrow \bar{I}^{(a)}_{1,2,3,4,7}, \qquad I^{(a)}_{5,6,8,9} \Rightarrow -\bar{I}^{(a)}_{5,6,8,9}. \quad (11)$$

Here $\bar{I}_i^{(a)}$ are the complex conjugate of $I_i^{(a)}$. Therefore, one can define twelve CP averaged angular observables as [4,5]

$$S_i^{(a)}(q^2) = \frac{I_i^{(a)}(q^2) + \bar{I}_i^{(a)}(q^2)}{d(\Gamma + \bar{\Gamma})/dq^2}, \quad (12)$$

along with twelve CP asymmetries

$$A_i^{(a)}(q^2) = \frac{I_i^{(a)}(q^2) - \bar{I}_i^{(a)}(q^2)}{d(\Gamma + \bar{\Gamma})/dq^2}. \quad (13)$$

The CP asymmetry in the dimuon mass spectrum is defined as

$$A_{CP}(q^2) = \frac{d\Gamma/dq^2 - d\bar{\Gamma}/dq^2}{d\Gamma/dq^2 + d\bar{\Gamma}/dq^2}, \quad (14)$$

where $d\Gamma/dq^2$ can be expressed in terms of angular coefficients as

$$\frac{d\Gamma}{dq^2} = \frac{3}{4}(2I_1^s + I_1^c) - \frac{1}{4}(2I_2^s + I_2^c). \quad (15)$$

Apart from A_{CP}, in this work we consider $A_{3,4,5}$, A_6^s and $A_{7,8,9}$ observables. These observables are measured by the LHCb collaboration, however, with large errors [15]. The angular observables $A_{3,4,5}$ and A_6^s are direct CP like asymmetries whereas $A_{7,8,9}$ are triple product CP asymmetries [4]. Therefore $A_{7,8,9}$ observables seem to be more sensitive to new weak phases as compared to the other observables.

First of all, we examine $A_{CP}^{K^*}$. Based on predictions obtained in Table III for various favored scenarios, it is pellucid that none of the solutions can enhance $A_{CP}^{K^*}$ to a level of a percent in the low-q^2 bin. Therefore, the current $b \to s\ell\ell$ data suggests that the measurement of A_{CP} in $B^0 \to K^{*0}\mu^+\mu^-$ decay in the low-q^2 region would be a formidable task. On the contrary, in the high-q^2 bin, all favored new physics scenarios can ameliorate $A_{CP}^{K^*}$ up to 2%–3%. However, as the maximum allowed value of $A_{CP[15-19]}^{K^*}$ for all solutions are close to each other, one needs to look for additional CP violating observables to discriminate between the allowed solutions.

TABLE III. Predictions of A_{CP} in $B^0 \to K^{*0}\mu^+\mu^-$ decay (1σ range). Here $A_{CP}^{K^*} \equiv A_{CP}(B^0 \to K^{*0}\mu^+\mu^-)$.

Wilson coefficients	$A_{CP[1-6]}^{K^*}$ (%)	$A_{CP[15-19]}^{K^*}$ (%)
$C_i = 0$ (SM)	≈0	≈0
1D scenarios:		
C_9^{NP}	(0.01, 0.11)	(−1.79, 1.78)
$C_9^{NP} = -C_{10}^{NP}$	(−0.04, 0.14)	(−2.69, 2.71)
$C_9^{NP} = -C_9'$	(−0.06, 0.14)	(−3.19, 3.09)

TABLE IV. Prediction of various CP violating angular observables (1σ range) in $B^0 \to K^{*0}\mu^+\mu^-$ in the low-q^2 region.

Wilson coefficient(s)	$A_{3[1-6]}$ (%)	$A_{4[1-6]}$ (%)	$A_{5[1-6]}$ (%)	$A^s_{6[1-6]}$ (%)	$A_{7[1-6]}$ (%)	$A_{8[1-6]}$ (%)	$A_{9[1-6]}$ (%)
$C_i = 0$ (SM)	≈ 0	≈ 0	≈ 0	≈ 0	≈ 0	≈ 0	≈ 0
1D scenarios:							
C_9^{NP}	(0.00, 0.01)	$(-0.10, 0.15)$	(0.04, 0.04)	$(-0.08, -0.07)$	(0.27, 0.29)	$(-3.03, 3.45)$	$(-0.31, 0.36)$
$C_9^{NP} = -C_{10}^{NP}$	$(-0.01, 0.02)$	$(-0.17, 0.23)$	$(-0.40, 0.49)$	$(-0.79, 0.60)$	$(-9.17, 10.38)$	$(-4.74, 5.34)$	$(-0.49, 0.55)$
$C_9^{NP} = -C_9'$	$(-0.24, 0.23)$	$(-0.24, 0.28)$	(0.04, 0,04)	$(-0.09, -0.08)$	(0.27, 0.32)	$(-0.91, 1.04)$	$(-0.21, 0.15)$

The predictions of several CP violating angular observables in $B^0 \to K^{*0}\mu^+\mu^-$ in the low and high-q^2 regions are exhibited in Table IV and V, respectively. From Table IV, it is unambivalent that all three allowed solutions predict $A_{3,4,5}$, A_6^s, and A_9 asymmetries to be less than a percent in the low-q^2 bin and hence making their observation an arduous endeavor. However, the prediction of observable A_7 provides encouraging sign for $C_9^{NP} = -C_{10}^{NP}$ solution for which $A_{7[1-6]}$ can be enhanced up to 10%. For all other solutions, $A_{7[1-6]} < 1\%$. Therefore the measurement of $A_{7[1-6]}$ observable can lead to a unique identification of new physics solution in the form of $C_9^{NP} = -C_{10}^{NP}$. The C_9^{NP} and $C_9^{NP} = -C_{10}^{NP}$ solutions can bolster $A_{8[1-6]}$ at the level of 4%–5% whereas for $C_9^{NP} = -C_9'$ scenario, $A_{8[1-6]} \lesssim 1\%$. Therefore measurement of $A_{8[1-6]}$ at the level of few percent would discriminate $C_9^{NP} = -C_9'$ new physics scenario from other two scenarios. As both C_9^{NP} and $C_9^{NP} = -C_{10}^{NP}$ solutions allow almost similar enhancement in the value of $A_{8[1-6]}$, a discrimination between these two solutions would not be possible through this observable.

We now consider predictions of A_i observables in the high-q^2 bin as given in Table V. The most conspicuous feature of predictions in the low-q^2 region was related to the observable A_7 which insinuated to be a potential observable to verbalize the signatures of weak phase related to the new physics solution $C_9^{NP} = -C_{10}^{NP}$. However, unlike in the low-q^2 bin, all allowed 1D solutions fail to provide an enhancement in A_7 above a percent level in the high-q^2 region. The $C_9^{NP} = -C_9'$ scenario failed to make any noticeable indentations in the low-q^2 bin as it was unable to provide any detectable enhancements in any of the considered A_i observables. However, in the high-q^2 bin, this solution appears to make a riveting impact as it can enhance A_8 and A_9 observables up to a level $\sim$(4–6)%. All other favored scenarios fail to provide any meaningful enhancement in these observables. This thus implies that the observation of either A_8 or A_9 asymmetries at the level of a few percent in the high-q^2 bin may provide confirmatory evidence in support of the $C_9^{NP} = -C_9'$ scenario.

The observable A_6^s failed to make any imprint in the low-q^2 bin. However in [15–19] bin, this can be enhanced up to $\sim$(2–3)% by $C_9^{NP} = -C_{10}^{NP}$ scenario. The other two scenarios predict $A_6^s < 1\%$. Therefore the observation of A_6^s in the high-q^2 bin at the level of a few percent would provide an unambiguous signature of new physics in the form of $C_9^{NP} = -C_{10}^{NP}$ solution. None of the 1D solutions in [1-6] bin provided any meaningful enhancements in $A_{3,4,5}$ angular observables. On the contrary, all of these observables can be enhanced up to a level of a few percent in the high-q^2 bin. The A_5 observable can be brought to a percent level by $C_9^{NP} = -C_{10}^{NP}$ solution. All solutions have the potential to bring A_4 observable up to a level of a percent or more. A similar job for $A_{3[15-19]}$ observable can be done by $C_9^{NP} = -C_{10}^{NP}$ and $C_9^{NP} = -C_9'$ solutions.

Thus we see that an accurate measurement of A_{CP} in the high-q^2 bin along with a number of CP violating angular observables would enable unique identification of possible new physics in $b \to s\ell\ell$ transition. This can be easily understood with the help of summary Table VI. In this table, we have listed those observables for which the current allowed solutions can provide meaningful enhancement, say values above 2%. For each new physics solutions, the observables are distributed in different blocks based on their allowed values.

TABLE V. Prediction of various CP violating angular observables (1σ range) in $B^0 \to K^{*0}\mu^+\mu^-$ in the high-q^2 region.

Wilson coefficient(s)	$A_{3[15-19]}$ (%)	$A_{4[15-19]}$ (%)	$A_{5[15-19]}$ (%)	$A^s_{6[15-19]}$ (%)	$A_{7[15-19]}$ (%)	$A_{8[15-19]}$ (%)	$A_{9[15-19]}$ (%)
$C_i = 0$ (SM)	≈ 0	≈ 0	≈ 0	≈ 0	≈ 0	≈ 0	≈ 0
1D scenarios:							
C_9^{NP}	$(-0.72, 0.73)$	$(-1.06, 1.07)$	(0.10, 0.11)	$(-0.21, -0.18)$	(0.01, 0.01)	$(-0.13, 0.15)$	$(-0.11, 0.13)$
$C_9^{NP} = -C_{10}^{NP}$	$(-1.11, 1.10)$	$(-1.62, 1.61)$	$(-1.51, 1.58)$	$(-2.79, 2.65)$	$(-0.40, 0.45)$	$(-0.20, 0.24)$	$(-0.17, 0.20)$
$C_9^{NP} = -C_9'$	$(-1.91, 1.91)$	$(-2.13, 2.17)$	(0.10, 0.12)	$(-0.22, -0.18)$	(0.01, 0.01)	$(-3.58, 3.56)$	$(-6.40, 6.33)$

TABLE VI. A plot exhibiting discriminating capabilities of various *CP* violating observables in $B^+ \to K^+\mu^+\mu^-$ and $B^0 \to K^{*0}\mu^+\mu^-$ decays. In each row, we show new physics solutions along with the observables where a meaningful enhancement is allowed. These observables are further classified in three categories on the basis of maximum amount of enhancements, $A^{\max}$, allowed by the current data. It is obvious that any observable which is placed in $A^{\max} \gtrsim 10\%$ or $A^{\max} \approx 5\%$–9% column also appears in the preceding columns. The observables marked in green color are termed as unique identifier of the specific new physics solution (appearing in the same row in which these observables appear), i.e., these observables will not appear in any other row. The observables marked in blue and red colors are degenerate observables in the sense that they appear in more than one row. Here and $A^L_{7,8} \equiv A_{7,8[1-6]}$ and $A^H_{4,6,8,9} \equiv A_{4,6,8,9[15-19]}$. Further, A^K_{CP} and $A^{K^*}_{CP}$ observables are in high-q^2 bin.

1D scenarios	$A^{\max} \approx (2$–$5)\%$	$A^{\max} \approx (5$–$9)\%$	$A^{\max} \gtrsim 10\%$
C_9^{NP}	A^K_{CP}, $A^{K^*}_{CP}$, A^L_8		
$C_9^{NP} = -C_{10}^{NP}$	$A^{K^*}_{CP}$, A^H_6	A^K_{CP}, A^L_8	A^L_7
$C_9^{NP} = -C'_9$	A^H_4, $A^{K^*}_{CP}$, A^H_8	A^H_9	

The observables represented in green color are unique identifiers. For, e.g., the observable $A_{7[1-6]}$ appears in all three blocks. This implies that the measurement of $A_{7[1-6]}$ with any value greater than 2% can provide confirmatory evidence for new physics in the form of $C_9^{NP} = -C_{10}^{NP}$ solution. Similarly, measurement of A_6^s in (2–5)% range would turn out to be another unique identifier of $C_9^{NP} = -C_{10}^{NP}$ scenario. For $C_9^{NP} = -C'_9$ solution, $A_{4,8,9}$ observables in the high-q^2 bin will serve this task. Further, the C_9^{NP} solution does not have any unique identifier, i.e., its confirmation would require measurements of more than one observable.

The observables represented by blue and red colors in Tab. VI provide signatures of new physics for multiple scenarios. The $A^{K^*}_{CP}$ in the high-q^2 bin is allowed to have values in the range of (2–5)% for all three scenarios. Similarly, A^K_{CP} in high-q^2 and A_8 in low-q^2 bin can be enhanced by C_9^{NP} as well as $C_9^{NP} = -C_{10}^{NP}$ scenarios. Therefore, a careful scrutinization is required to see whether these observables in combination with others can also provide unique identification. It is apparent from the table that the following combinations can also serve as a useful discriminant for new physics solutions:

(i) $[A^K_{CP}$-$A^{K^*}_{CP}]$ in high-q^2: A simultaneous measurement of these observables can be used as a good discriminant for $C_9^{NP} = -C'_9$ solution. The C_9^{NP} as well as $C_9^{NP} = -C_{10}^{NP}$ solutions allow both of these observables to have values greater than 2% whereas the $C_9^{NP} = -C'_9$ scenario doesn't allow any meaningful enhancement in A^K_{CP}. Therefore any measurement of both A^K_{CP} and $A^{K^*}_{CP}$ in high-q^2 region at the level of few percent would disfavor $C_9^{NP} = -C'_9$ scenario. The same is corroborated from the correlation plot between these observables as depicted in the left panel of Fig. 2. It is obvious that both A^K_{CP} and $A^{K^*}_{CP}$ enjoy positive correlations with each other for C_9^{NP} and $C_9^{NP} = -C_{10}^{NP}$ solutions, i.e., a finite measurement of one observable would imply the same for the other whereas for $C_9^{NP} = -C'_9$ scenario, a finite value of $A^{K^*}_{CP}$ implies $A^K_{CP} \approx 0$ in the entire high-q^2 bin.

(ii) $A_{8[1-6]}$-$A^{K^*}_{CP}$ (high-q^2): A simultaneous measurement of these observables can discriminate between $C_9^{NP} = -C'_9$ solution with others. The other two solutions allow meaningful enhancements in both of these observables whereas $C_9^{NP} = -C'_9$ solution can boost only $A^{K^*}_{CP}$ in the high-q^2 bin. This feature is also reflected from the right panel of Fig. 2.

For a finer scrutinization of possible new physics contributions to $b \to s\ell\ell$, we now investigate other correlations between A_{CP} and *CP* violating angular observables A_i's in $B^0 \to K^{*0}\mu^+\mu^-$. We first examine these correlations between A^K_{CP} in the high-q^2 bin and $A_{7,8[1-6]}$ as for all other angular observables in the low-q^2 region, enhancements are too small to be observed. Further, we do not consider $A_{7,8[1-6]}$ correlations with A^K_{CP} in the low-q^2 bin as $A^K_{CP} < 1\%$ in this bin. These correlations are vignetted in Fig. 3. For $C_9^{NP} = -C_{10}^{NP}$ solution, A^K_{CP} and $A_{7[1-6]}$ observables are correlated in the sense that the larger enhancement in A^K_{CP} will commensurate a larger enhancement in $A_{7[1-6]}$ as well. For, e.g., for $A^K_{CP} \approx 5\%$, $A_{7[1-6]}$ can be $\sim$10%. For C_9^{NP} solution, $A_{7[1-6]} < 1\%$ for the entire allowed range of A^K_{CP} and both of these observables remain unstirred for the $C_9^{NP} = -C'_9$ solution.

The correlations between A^K_{CP} in the high-q^2 bin and $A_{8[1-6]}$ are explicated in the right panel of Fig. 3. For $C_9^{NP} = -C_{10}^{NP}$ scenario, the maximum possible enhancement in $A^K_{CP} \approx 5\%$ can be accustomed with the maximum allowed

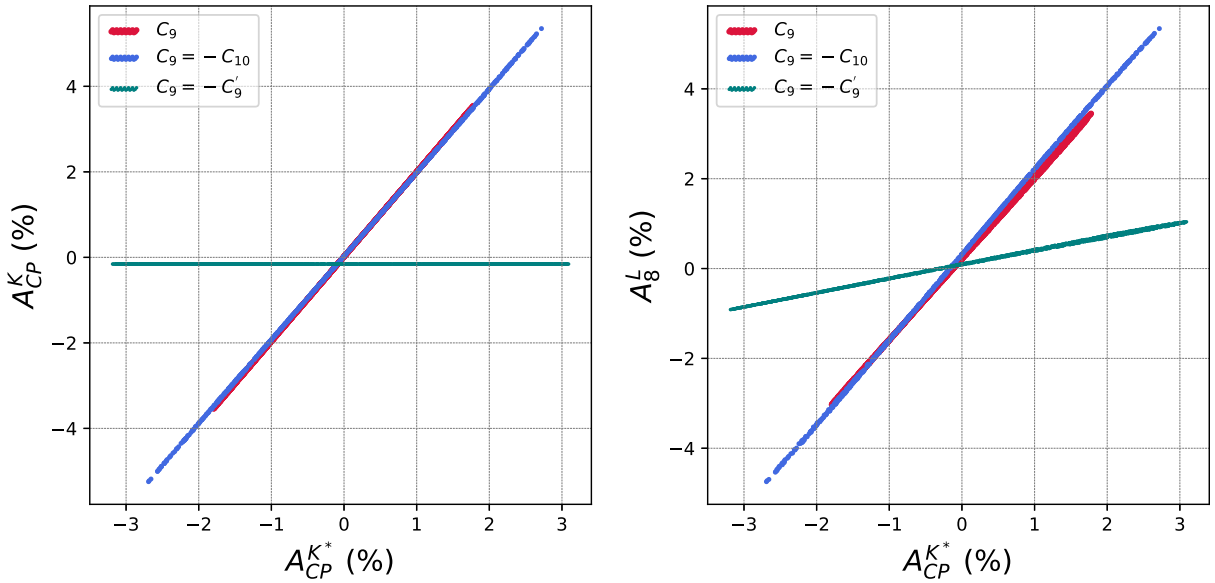

FIG. 2. The left panel portrays correlations between A_{CP} in $B^0 \to K^{*0}\mu^+\mu^-$ and $B^+ \to K^+\mu^+\mu^-$ in the high-q^2 region for all favored "1D" solutions. A correlation between A_{CP} in $B^0 \to K^{*0}\mu^+\mu^-$ in the high-q^2 bin and A_8 observable in the low-q^2 region (A_8^L) is depicted in the right panel.

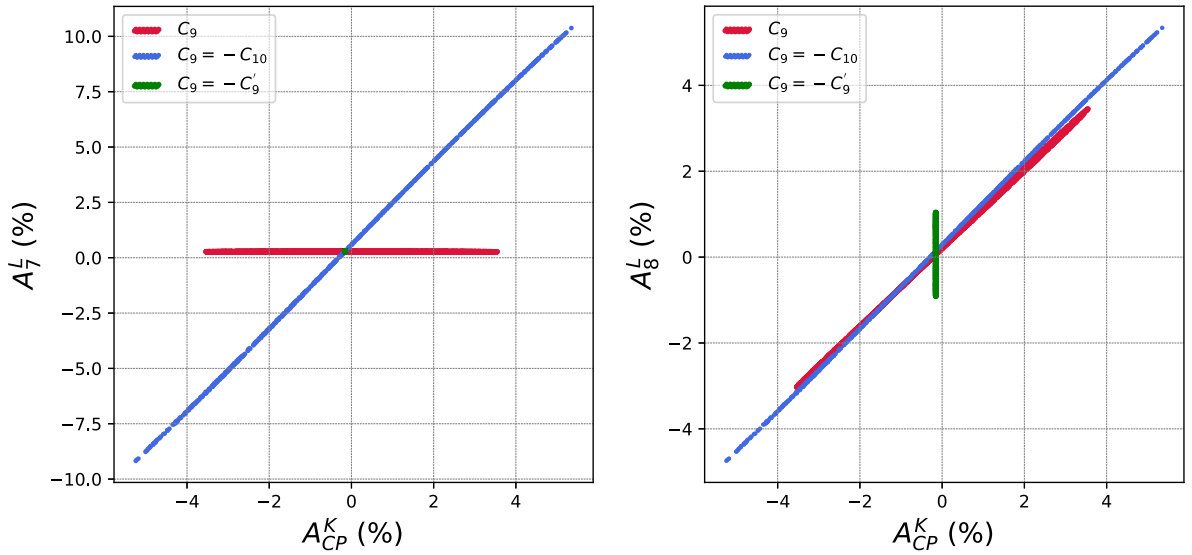

FIG. 3. The left panel portrays correlations between A_{CP} in $B^+ \to K^+\mu^+\mu^-$ in the high-q^2 and A_7 observable in the low-q^2 region for all favored "1D" solutions. A correlation between A_{CP} in $B^+ \to K^+\mu^+\mu^-$ in the high-q^2 bin and A_8 observable in the low-q^2 region is depicted in the right panel.

value of $A_{8[1-6]} \approx 5\%$ and vice-versa. For C_9^{NP} scenario, $A_{8[1-6]}$ and A_{CP}^K have positive correlations and their behavior is identical to that of $C_9^{NP} = -C_{10}^{NP}$ solution but with slightly smaller enhancement ($\approx$3%) in both observables. The A_{CP}^K remains unaltered for the $C_9^{NP} = -C_9'$ solution with $\leq 1\%$ enhancement in $A_{8[1-6]}$ observable.

We now delve correlations in the high-q^2 region. The interrelations between $A_{CP}^{K^*}$ and A_i are demonstrated in Fig. 4. Here we do not consider A_7 observable as none of the allowed 1D scenarios can enhance it up to a level of a percent. The $(A_{CP}^{K^*} - A_3)$ and $(A_{CP}^{K^*} - A_4)$ correlations are almost similar. These CP violating angular observables are anti-correlated with $A_{CP}^{K^*}$ for the three allowed solutions, i.e., a negative value of $A_{CP}^{K^*}$ would imply $A_{3,4} > 0$ and vice versa. Further, $|A_{CP}^{K^*}| \approx 3\%$, which is the maximum allowed value of $A_{CP}^{K^*}$ with the current data, can lead to $|A_{3,4}| \approx 2\%$ for $C_9^{NP} = -C_9'$ scenario. For C_9^{NP} and $C_9^{NP} = -C_{10}^{NP}$ scenarios, $A_{CP}^{K^*\max}$ implies $A_{3,4} \approx 1\%$.

From $(A_{CP}^{K^*} - A_{5,6}^{(s)})$ plots, it is obvious that A_5 (A_6^s) has negative (positive) correlations with $A_{CP}^{K^*}$ for $C_9^{NP} = -C_{10}^{NP}$

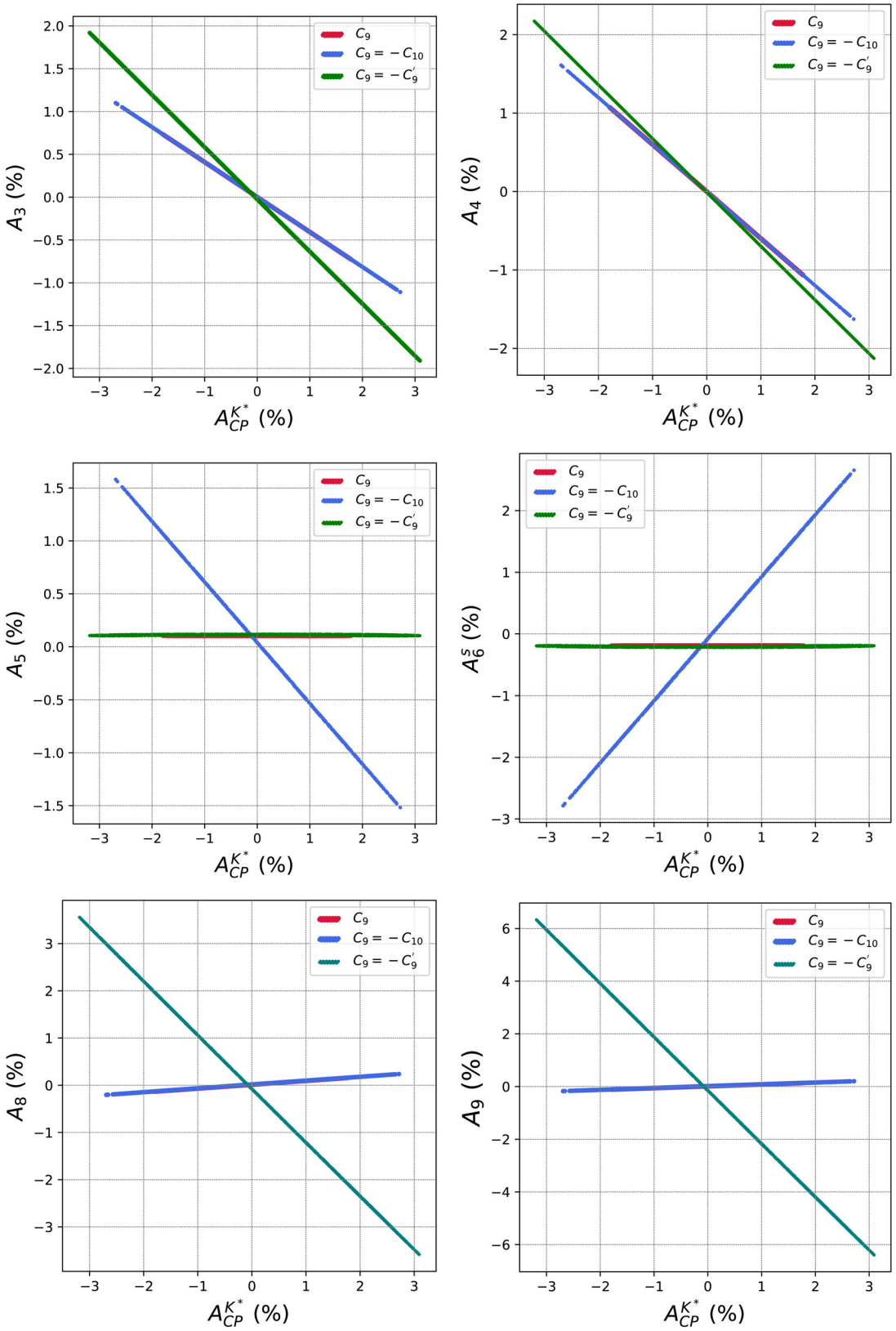

FIG. 4. These plots reveal correlations between A_{CP} in $B^0 \to K^{*0}\mu^+\mu^-$ and several A_i observables for all favored "1D" solutions in the high-q^2 bin.

solution. For, e.g., a measurement of $A_{CP}^{K^*}$ with a value $\approx -3\%$ would lead to an observation of A_5 (A_6^s) with a value $\approx 1\%$ ($\approx -2\%$). Therefore simultaneous measurements of $A_{CP}^{K^*}$ and $A_{5,6}^{(s)}$ can discriminate $C_9^{NP} = -C_{10}^{NP}$ solution from others. The $(A_{CP}^{K^*} - A_8)$ and $(A_{CP}^{K^*} - A_9)$ correlations features are almost similar for the three scenarios. Here $A_{8,9}$ have anti-correlations with $A_{CP}^{K^*}$ for the $C_9^{NP} = -C_9'$ scenario. For this solution, a measurement of $A_{CP}^{K^*} \approx -3\%$ would imply $A_{8,9} \approx 5\%$.

As of now, we have been emphasizing on the measurements of the angular observables A_i along with A_{CP}'s for discriminating between the allowed solutions. However, these correlations will also be helpful in discarding or identifying a particular scenario with a precise measurement of A_{CP} even if we only have upper bounds on the A_i observables. For e.g., from $(A_{CP}^{K^*} - A_8)$ correlation plot in the high-q^2 region, it is evident that a finite value of $A_{CP}^{K^*}$ indicates a finite value of A_8 for $C_9^{NP} = -C_9'$ scenario. In case, the experimental upper bounds on A_8 slips below the value predicted by the correlation plot (on the basis of the measured value of $A_{CP}^{K^*}$), the given scenario would be disfavored.

This may also help in the identification of C_9^{NP} solution. As evident from the left panel of Fig. 2, for this solution (as well as $C_9^{NP} = -C_{10}^{NP}$), A_{CP}^{K} and $A_{CP}^{K^*}$ in the high-q^2 have positive correlation, i.e., a larger value in one will imply the same for other observable. Therefore if both of these observables are measured, say with a value $\gtrsim 2\%$, this can only be due to either C_9^{NP} or $C_9^{NP} = -C_{10}^{NP}$ scenario. This degeneracy can be removed by inspecting correlations of A_{CP} with A_i observables. For e.g., ($A_{CP}^{K^*}$-A_6^s) plot predicts $|A_6^s| \approx 2\%$ for $C_9^{NP} = -C_{10}^{NP}$ solution corresponding to $|A_{CP}^{K^*}| \approx 2\%$ and ≈ 0 for C_9^{NP} scenario. Therefore if the experimental upper bound on $|A_6^s|$ observable falls below 2%, such a scenario can only be accommodated by the C_9^{NP} solution.

On similar lines, the simultaneous measurements of A_{CP}^{K} and $A_{CP}^{K^*}$ in the high-q^2 bins can be used as a good identifier between the possible NP solutions. In case, $A_{CP}^{K^*}$ is measured at the level of $\gtrsim 2\%$ and the upper bounds on A_{CP}^{K} shrinks to less than 2%, it would be enough to identify $C_9^{NP} = -C_9'$ solution by disfavoring the other two.

V. CONCLUSIONS

Assuming new physics Wilson coefficients to be complex, we perform a model-independent global fit to all apropos $b \to s\ell\ell$ ($\ell = e,\ \mu$) data. This include updated measurements of R_K and R_{K^*} by the LHCb collaboration in December 2022 together with the updated measurement of the branching ratio of $B_s \to \mu^+\mu^-$ by the CMS collaboration and the measurements of several $B_s \to \phi\mu^+\mu^-$ observables. We work under the assumption that the new physics equally affects both the muon and electron sectors. For comparison, we also update the fits for real couplings under the assumption of universal couplings. Considering only one operator or two related operators at a time, we obtain the following:

(i) The allowed solutions remain the same as obtained for the real fits, i.e., $C_9^{\rm NP}$, $C_9^{\rm NP} = -C_{10}^{\rm NP}$ and $C_9^{NP} = -C_9'$ scenarios still provide a good or moderate fits to the data.

(ii) The $C_9^{\rm NP}$ and $C_9^{NP} = -C_9'$ scenarios now becomes the most preferred one as the $\Delta\chi^2$ for $C_9^{\rm NP} = -C_{10}^{\rm NP}$ solution falls by ~ 10 below $\Delta\chi^2$ values for the other two scenarios. Therefore the $C_9^{\rm NP} = -C_{10}^{\rm NP}$ scenario can only be considered as a moderate solution.

(iii) The $C_{10}^{\rm NP}$ scenario which provided a moderate fit to the data before CMS and December 2022 LHCb updates now fails to provide any significant improvement in the value of $\Delta\chi^2$.

We find that the current data allows complex couplings to exist with an upper bound similar to that of their real counterparts. The effect of such a weak phase can show up in some of the CP asymmetries. For the favored solutions, we obtain predictions of several CP-violating observables in $B^0 \to K^{*0}\mu^+\mu^-$ and direct CP asymmetry in $B^+ \to K^+\mu^+\mu^-$. These asymmetries can be observed at the current or planned experimental facilities provided new physics enhances them up to a level of a few percent. Following are our main observations:

(i) None of the new physics solutions can enhance A_{CP} in the low-q^2 bin at the level of a few percent. Such an enhancement is feasible only in the high-q^2 region. This is true for $B^+ \to K^+\mu^+\mu^-$ as well as $B^0 \to K^{*0}\mu^+\mu^-$ decay. For $B^+ \to K^+\mu^+\mu^-$, such an enhancement can be provided by C_9^{NP} or $C_9^{NP} = -C_{10}^{NP}$ solutions, the enhancement being more pronounced for the later solution. For $B^0 \to K^{*0}\mu^+\mu^-$ decay, all solutions can serve this purpose.

(ii) All allowed solutions predict $A_{3,4,5}$, A_6^s and A_9 asymmetries to be less than a percent level in the low-q^2 bin. However, the predictions of observable A_7 provides eupeptic sign for $C_9^{NP} = -C_{10}^{NP}$ solution as $A_{7[1\text{–}6]}$ can be enhanced up to 10%. Therefore $A_{7[1\text{–}6]}$ can be termed as an unique identifier for $C_9^{NP} = -C_{10}^{NP}$ solution.

(iii) The C_9^{NP} and $C_9^{NP} = -C_{10}^{NP}$ solutions can bolster $A_{8[1\text{–}6]}$ at the level of 4–5%.

(iv) The observation of any of the A_4, A_8 or A_9 observables at a level of a few percent in the high-q^2 bin may provide confirmatory evidence in support of the $C_9^{NP} = -C_9'$ scenario.

(v) The observable $A_{3,4,5}$ and A_6^s failed to make any impact in the low-q^2 bin. However in [15–19] bin, all of these observables can be enhanced up to a level of a percent or more. A measurement of A_6^s up to (2–3)% level would provide unique identification of $C_9^{NP} = -C_{10}^{NP}$ solution.

Finally, we study correlations between A_{CP} and other CP asymmetries. Our findings are as follows:

(i) A simultaneous measurement of A_{CP}^{K} and $A_{CP}^{K^*}$ in the high-q^2 bin can be used as a good discriminant for $C_9^{NP} = -C_9'$ solution. The same can also be achieved by simultaneous measurements of $A_{8\,[1\text{–}6]}$ and $A_{CP}^{K^*}$ in the high-q^2 region.

(ii) The $(A_{CP}^{K^*} - A_3)$ and $(A_{CP}^{K^*} - A_4)$ correlations in the high-q^2 bin cannot discriminate between any of the solutions whereas a simultaneous measurement of $A_{CP}^{K^*}$ and A_5 (or A_6^s) in high-q^2 region can distinguish $C_9^{NP} = -C_{10}^{NP}$ from other scenarios. A similar identification for $C_9^{NP} = -C_9'$ solution can be provided by examining $(A_{CP}^{K^*} - A_{8,9})$ correlations in the high-q^2 bin.

(iii) If A_{CP} is precisely measured in the high-q^2 region, the new physics solutions can also be identified even if we only have upper bounds on the A_i observables. For some scenarios, a discrimination would be possible only through $(A_{CP}^{K}$-$A_{CP}^{K^*})$ correlations in the high-q^2 bin.

Therefore the observation of A_{CP} as well as CP violating angular observables will not only provide an evidence of new physics with complex phase but their accurate measurements would also facilitate the unique identification of possible new physics in the decays induced by the $b \to s\ell\ell$ transition. The direct CP asymmetry can be measured at the LHCb or Belle-II, however the measurements of CP violating angular observables require higher statistics which can be attained at the HL-LHC [83].

ACKNOWLEDGMENTS

I would like to thank Roman Zwicky for useful suggestions. I would also like to thank Arindam Mandal and Ashutosh Kumar Alok for helpful discussions on various aspects of the draft.

APPENDIX A: DECAY RATE OF $B \to K\mu^+\mu^-$ DECAY

The decay rate of $B \to K\mu^+\mu^-$ is given by [84,85]

$$\Gamma(B \to K\mu^+\mu^-) = \int_{q^2_{\rm min}}^{q^2_{\rm max}} dq^2 \left(2a_\mu(q^2) + \frac{2}{3}c_\mu(q^2)\right), \quad \text{(A1)}$$

where

$$a_\mu(q^2) = E(q^2)\Big[q^2|F_P|^2 + \frac{\lambda}{4}(|F_V|^2 + |F_A|^2) + 2m_\mu(m_B^2 - m_K^2 + q^2)\mathrm{Re}(F_P F_A^*) + 4m_\mu^2 m_B^2 |F_A|^2\Big], \quad \text{(A2)}$$

$$c_\mu(q^2) = -\frac{\lambda}{4}\beta_\mu^2 E(q^2)(|F_V|^2 + |F_A|^2), \quad \text{(A3)}$$

with

$$E(q^2) = \frac{G_F^2 \alpha |V_{tb}V_{ts}^*|^2}{512\pi^5 m_B^3}\beta_\mu \lambda_K. \quad \text{(A4)}$$

Here $\lambda = m_B^4 + m_K^4 + q^4 - 2(m_B^2 m_K^2 + m_B^2 q^2 + m_K^2 q^2)$ and $\beta_\mu = \sqrt{1 - 4m_\mu^2/q^2}$. In the low-$q^2$ region, all form-factors reduce to one soft form-factor [86,87]. In the high-q^2 region too, symmetry relations among the form factors can be delved with the improved Isgur-Wise relation [88].

APPENDIX B: ANGULAR COEFFICIENTS IN $B^0 \to K^{*0}\mu^+\mu^-$ DECAY

The angular coefficients appearing in the four-fold distribution of $B \to K^*(\to K\pi)\mu^+\mu^-$ decay can be expressed in terms of transversity amplitudes as [5]

$$\begin{aligned}
I_1^s &= \frac{(2+\beta_\mu^2)}{4}\Big[|A_\perp^L|^2 + |A_\parallel^L|^2 + (L \to R)\Big] + \frac{4m_\mu^2}{q^2}\mathrm{Re}(A_\perp^L A_\perp^{R*} + A_\parallel^L A_\parallel^{R*}),\\
I_1^c &= |A_0^L|^2 + |A_0^R|^2 + \frac{4m_\mu^2}{q^2}[|A_t|^2 + 2\mathrm{Re}(A_0^L A_0^{R*})],\\
I_2^s &= \frac{\beta_\mu^2}{4}\Big[|A_\perp^L|^2 + |A_\parallel^L|^2 + (L \to R)\Big],\\
I_2^c &= -\beta_\mu^2\Big[|A_0^L|^2 + |A_0^R|^2\Big],\\
I_3 &= \frac{\beta_\mu^2}{2}\Big[|A_\perp^L|^2 - |A_\parallel^L|^2 + (L \to R)\Big],\\
I_4 &= \frac{\beta_\mu^2}{\sqrt{2}}\Big[\mathrm{Re}(A_0^L A_\parallel^{L*}) + (L \to R)\Big],\\
I_5 &= \sqrt{2}\beta_\mu\Big[\mathrm{Re}(A_0^L A_\perp^{L*}) - (L \to R)\Big],\\
I_6^s &= 2\beta_\mu\Big[\mathrm{Re}(A_\parallel^L A_\perp^{L*}) - (L \to R)\Big],\\
I_7 &= \sqrt{2}\beta_\mu\Big[\mathrm{Im}(A_0^L A_\parallel^{L*}) - (L \to R)\Big],\\
I_8 &= \frac{\beta_\mu^2}{\sqrt{2}}\Big[\mathrm{Im}(A_0^L A_\perp^{L*}) + (L \to R)\Big],\\
I_9 &= \beta_\mu^2\Big[\mathrm{Im}(A_\parallel^{L*} A_\perp^L) + (L \to R)\Big].
\end{aligned} \quad \text{(B1)}$$

The expressions of transversity amplitudes can be found in Ref. [5,73]. These amplitudes are written in terms of form-factors $V(q^2)$, $A_{0,1,2}(q^2)$ and $T_{1,2,3}(q^2)$. The hadronic uncertainties in $B \to K^*\ell^+\ell^-$ observables are mainly

due to form-factors [73,74,89] and nonlocal contributions related with charm-quark loops [89–96]. The form-factors in the low-q^2 region are calculated using light-cone sum rules (LCSR) or light-meson distribution amplitudes. In the high-q^2 region, the form-factors are determined from lattice computations [97,98].

[1] A. D. Sakharov, Pis'ma Zh. Eksp. Teor. Fiz. **5**, 32 (1967).
[2] F. Kruger, L. M. Sehgal, N. Sinha, and R. Sinha, Phys. Rev. D **61**, 114028 (2000); **63**, 019901(E) (2001).
[3] F. Kruger and E. Lunghi, Phys. Rev. D **63**, 014013 (2001).
[4] C. Bobeth, G. Hiller, and G. Piranishvili, J. High Energy Phys. 07 (2008) 106.
[5] W. Altmannshofer, P. Ball, A. Bharucha, A. J. Buras, D. M. Straub, and M. Wick, J. High Energy Phys. 01 (2009) 019.
[6] C. Bobeth, G. Hiller, and D. van Dyk, J. High Energy Phys. 07 (2011) 067.
[7] A. K. Alok, A. Datta, A. Dighe, M. Duraisamy, D. Ghosh, and D. London, J. High Energy Phys. 11 (2011) 122.
[8] S. N. Gangal, arXiv:2209.02476.
[9] D. Das, J. Das, G. Kumar, and N. Sahoo, arXiv:2211.09065.
[10] C. Q. Geng, C. W. Liu, and Z. Y. Wei, arXiv:2212.02976.
[11] R. Fleischer, E. Malami, A. Rehult, and K. K. Vos, J. High Energy Phys. 03 (2023) 113.
[12] R. Aaij *et al.* (LHCb Collaboration), J. High Energy Phys. 09 (2015) 179.
[13] R. Aaij *et al.* (LHCb Collaboration), Phys. Rev. Lett. **127**, 151801 (2021).
[14] R. Aaij *et al.* (LHCb Collaboration), Phys. Rev. Lett. **111**, 191801 (2013).
[15] R. Aaij *et al.* (LHCb Collaboration), J. High Energy Phys. 02 (2016) 104.
[16] R. Aaij *et al.* (LHCb Collaboration), Phys. Rev. Lett. **125**, 011802 (2020).
[17] S. Descotes-Genon, T. Hurth, J. Matias, and J. Virto, J. High Energy Phys. 05 (2013) 137.
[18] J. Matias and N. Serra, Phys. Rev. D **90**, 034002 (2014).
[19] L. Hofer and J. Matias, J. High Energy Phys. 09 (2015) 104.
[20] M. Ciuchini, M. Fedele, E. Franco, S. Mishima, A. Paul, L. Silvestrini, and M. Valli, J. High Energy Phys. 06 (2016) 116.
[21] T. Hurth, F. Mahmoudi, and S. Neshatpour, Nucl. Phys. **B909**, 737 (2016).
[22] M. Ciuchini, M. Fedele, E. Franco, A. Paul, L. Silvestrini, and M. Valli, Eur. Phys. J. C **83**, 64 (2023).
[23] M. Ciuchini, M. Fedele, E. Franco, A. Paul, L. Silvestrini, and M. Valli, Phys. Rev. D **107**, 055036 (2023).
[24] R. Aaij *et al.* (LHCb Collaboration), Phys. Rev. D **105**, 012010 (2022).
[25] ATLAS Collaboration, Report No. ATLAS-CONF-2020-049.
[26] M. Aaboud *et al.* (ATLAS Collaboration), J. High Energy Phys. 04 (2019) 098.
[27] A. M. Sirunyan *et al.* (CMS Collaboration), J. High Energy Phys. 04 (2020) 188.
[28] R. Aaij *et al.* (LHCb Collaboration), Phys. Rev. Lett. **118**, 191801 (2017).
[29] CMS Collaboration, Report No. CMS-PAS-BPH-21-006.
[30] Y. Amhis *et al.* (HFLAV Collaboration), Phys. Rev. D **107**, 052008 (2023).
[31] C. Bobeth, M. Gorbahn, T. Hermann, M. Misiak, E. Stamou, and M. Steinhauser, Phys. Rev. Lett. **112**, 101801 (2014).
[32] M. Bona *et al.* (UTfit Collaboration), arXiv:2212.03894.
[33] M. Bordone, G. Isidori, and A. Pattori, Eur. Phys. J. C **76**, 440 (2016).
[34] G. Hiller and F. Kruger, Phys. Rev. D **69**, 074020 (2004).
[35] R. Aaij *et al.* (LHCb Collaboration), Nat. Phys. **18**, 277 (2022).
[36] R. Aaij *et al.* (LHCb Collaboration), J. High Energy Phys. 08 (2017) 055.
[37] G. Isidori, S. Nabeebaccus, and R. Zwicky, J. High Energy Phys. 12 (2020) 104.
[38] G. Isidori, D. Lancierini, S. Nabeebaccus, and R. Zwicky, J. High Energy Phys. 10 (2022) 146.
[39] S. Nabeebaccus and R. Zwicky, Proc. Sci. CKM2021 (**2023**) 071.
[40] LHCb Collaboration, arXiv:2212.09152.
[41] LHCb Collaboration, arXiv:2212.09153.
[42] R. Aaij *et al.* (LHCb Collaboration), Phys. Rev. Lett. **128**, 191802 (2022).
[43] S. Descotes-Genon, J. Matias, and J. Virto, Phys. Rev. D **88**, 074002 (2013).
[44] W. Altmannshofer and D. M. Straub, Eur. Phys. J. C **73**, 2646 (2013).
[45] T. Hurth and F. Mahmoudi, J. High Energy Phys. 04 (2014) 097.
[46] B. Capdevila, S. Descotes-Genon, J. Matias, and J. Virto, J. High Energy Phys. 10 (2016) 075.
[47] M. Ciuchini, A. M. Coutinho, M. Fedele, E. Franco, A. Paul, L. Silvestrini, and M. Valli, Eur. Phys. J. C **77**, 688 (2017).
[48] A. K. Alok, B. Bhattacharya, D. Kumar, J. Kumar, D. London, and S. U. Sankar, Phys. Rev. D **96**, 015034 (2017).
[49] A. K. Alok, A. Dighe, S. Gangal, and D. Kumar, J. High Energy Phys. 06 (2019) 089.
[50] W. Altmannshofer and P. Stangl, Eur. Phys. J. C **81**, 952 (2021).
[51] A. Carvunis, F. Dettori, S. Gangal, D. Guadagnoli, and C. Normand, J. High Energy Phys. 12 (2021) 078.
[52] M. Algueró, B. Capdevila, S. Descotes-Genon, J. Matias, and M. Novoa-Brunet, Eur. Phys. J. C **82**, 326 (2022).
[53] L. S. Geng, B. Grinstein, S. Jäger, S. Y. Li, J. Martin Camalich, and R. X. Shi, Phys. Rev. D **104**, 035029 (2021).
[54] T. Hurth, F. Mahmoudi, D. M. Santos, and S. Neshatpour, Phys. Lett. B **824**, 136838 (2022).

[55] A. Angelescu, D. Bečirević, D. A. Faroughy, F. Jaffredo, and O. Sumensari, Phys. Rev. D **104**, 055017 (2021).
[56] A. K. Alok, N. R. Singh Chundawat, S. Gangal, and D. Kumar, Eur. Phys. J. C **82**, 967 (2022).
[57] N. R. Singh Chundawat, Phys. Rev. D **107**, 055004 (2023).
[58] R. Aaij *et al.* (LHCb Collaboration), J. High Energy Phys. 11 (2021) 043.
[59] R. Aaij *et al.* (LHCb Collaboration), Phys. Rev. Lett. **113**, 151601 (2014).
[60] D. M. Straub, arXiv:1810.08132.
[61] A. Abdesselam *et al.* (Belle Collaboration), Phys. Rev. Lett. **126**, 161801 (2021).
[62] J. P. Lees *et al.* (*BABAR* Collaboration), Phys. Rev. Lett. **112**, 211802 (2014).
[63] R. Aaij *et al.* (LHCb Collaboration), J. High Energy Phys. 11 (2016) 047.
[64] V. Khachatryan *et al.* (CMS Collaboration), Phys. Lett. B **753**, 424 (2016).
[65] CDF Collaboration, Updated branching ratio measurements of exclusive $b \to s\mu^+\mu^-$ decays and angular analysis in $B \to K^{(*)}\mu^+\mu^-$ decays, CDF public note 10894.
[66] R. Aaij *et al.* (LHCb Collaboration), J. High Energy Phys. 06 (2014) 133.
[67] M. Aaboud *et al.* (ATLAS Collaboration), J. High Energy Phys. 10 (2018) 047.
[68] A. M. Sirunyan *et al.* (CMS Collaboration), Phys. Lett. B **781**, 517 (2018).
[69] R. Aaij *et al.* (LHCb Collaboration), Phys. Rev. Lett. **126**, 161802 (2021).
[70] R. Aaij *et al.* (LHCb Collaboration), J. High Energy Phys. 04 (2015) 064.
[71] S. Wehle *et al.* (Belle Collaboration), Phys. Rev. Lett. **118**, 111801 (2017).
[72] F. James and M. Roos, Comput. Phys. Commun. **10**, 343 (1975).
[73] A. Bharucha, D. M. Straub, and R. Zwicky, J. High Energy Phys. 08 (2016) 098.
[74] N. Gubernari, A. Kokulu, and D. van Dyk, J. High Energy Phys. 01 (2019) 150.
[75] A. Datta and D. London, Phys. Lett. B **595**, 453 (2004).
[76] J. T. Wei *et al.* (Belle Collaboration), Phys. Rev. Lett. **103**, 171801 (2009).
[77] J. P. Lees *et al.* (*BABAR* Collaboration), Phys. Rev. D **86**, 032012 (2012).
[78] R. Aaij *et al.* (LHCb Collaboration), J. High Energy Phys. 09 (2014) 177.
[79] R. Aaij *et al.* (LHCb Collaboration), Phys. Rev. Lett. **110**, 031801 (2013).
[80] R. Aaij *et al.* (LHCb Collaboration), Phys. Rev. Lett. **111**, 151801 (2013).
[81] E. Kou *et al.* (Belle-II Collaboration), Prog. Theor. Exp. Phys. **2019**, 123C01 (2019); **2020**, 029201(E) (2020).
[82] J. Gratrex, M. Hopfer, and R. Zwicky, Phys. Rev. D **93**, 054008 (2016).
[83] A. Cerri, V. V. Gligorov, S. Malvezzi, J. Martin Camalich, J. Zupan, S. Akar, J. Alimena, B. C. Allanach, W. Altmannshofer, L. Anderlini *et al.*, CERN Yellow Rep. Monogr. **7**, 867 (2019).
[84] D. Becirevic, N. Kosnik, F. Mescia, and E. Schneider, Phys. Rev. D **86**, 034034 (2012).
[85] C. Bobeth, G. Hiller, and G. Piranishvili, J. High Energy Phys. 12 (2007) 040.
[86] J. Charles, A. Le Yaouanc, L. Oliver, O. Pene, and J. C. Raynal, Phys. Rev. D **60**, 014001 (1999).
[87] M. Beneke and T. Feldmann, Nucl. Phys. **B592**, 3 (2001).
[88] C. Bobeth, G. Hiller, D. van Dyk, and C. Wacker, J. High Energy Phys. 01 (2012) 107.
[89] A. Khodjamirian, T. Mannel, A. A. Pivovarov, and Y. M. Wang, J. High Energy Phys. 09 (2010) 089.
[90] M. Beneke, T. Feldmann, and D. Seidel, Nucl. Phys. **B612**, 25 (2001).
[91] S. Descotes-Genon, L. Hofer, J. Matias, and J. Virto, J. High Energy Phys. 12 (2014) 125.
[92] B. Capdevila, S. Descotes-Genon, L. Hofer, and J. Matias, J. High Energy Phys. 04 (2017) 016.
[93] C. Bobeth, M. Chrzaszcz, D. van Dyk, and J. Virto, Eur. Phys. J. C **78**, 451 (2018).
[94] T. Blake, U. Egede, P. Owen, K. A. Petridis, and G. Pomery, Eur. Phys. J. C **78**, 453 (2018).
[95] N. Gubernari, D. van Dyk, and J. Virto, J. High Energy Phys. 02 (2021) 088.
[96] N. Gubernari, M. Reboud, D. van Dyk, and J. Virto, J. High Energy Phys. 09 (2022) 133.
[97] R. R. Horgan, Z. Liu, S. Meinel, and M. Wingate, Phys. Rev. D **89**, 094501 (2014).
[98] J. Flynn, A. Jüttner, T. Kawanai, E. Lizarazo, and O. Witzel, Proc. Sci. LATTICE2015 (**2016**) 345.